Data-Centric Engineering (2025), 6: e39
doi:10.1017/dce.2025.10019

CAMBRIDGE UNIVERSITY PRESS

RESEARCH ARTICLE

OpenLimbTT, a transtibial residual limb shape model for prosthetics simulation and design: creating a statistical anatomic model using sparse data

Fiona Sunderland[1], Adam Sobey[2,3], Jennifer Bramley[1,4], Joshua Steer[1,4], Rami Al-Dirini[5], Cheryl Metcalf[6], Diana Toderita[7], Anthony Bull[7], Ziyun Ding[7,8], David Henson[7], the OpenLimb Group, Peter Worsley[9] and Alex Dickinson[1]

[1]Bioengineering Science Research Group, Faculty of Engineering and Physical Sciences, University of Southampton, Southampton, UK
[2]Data-Centric Engineering, The Alan Turing Institute, London, UK
[3]Maritime Engineering Research Group, Faculty of Engineering and Physical Sciences, University of Southampton, Southampton, UK
[4]Radii Devices Ltd., Bristol, UK
[5]Medical Device Research Institute, College of Science and Engineering, Flinders University, Adelaide, SA, Australia
[6]School of Healthcare Enterprise and Innovation, Faculty of Medicine, University of Southampton, Southampton, UK
[7]Department of Bioengineering, Imperial College London, London, UK
[8]Department of Mechanical Engineering, University of Birmingham, Birmingham, UK
[9]Skin Sensing Research Group, School of Health Sciences, Faculty of Environment and Life Sciences, University of Southampton, Southampton, UK
Corresponding author: Alex Dickinson; Email: alex.dickinson@soton.ac.uk

Received: 29 August 2024; **Revised:** 13 June 2025; **Accepted:** 03 July 2025

Keywords: principal component analysis; prosthetic limb; sparse data; statistical shape model; transtibial amputation

Abstract

Poor socket fit is the leading cause of prosthetic limb discomfort. However, currently clinicians have limited objective data to support and improve socket design. Finite element analysis predictions might help improve the fit, but this requires internal and external anatomy models. While external 3D surface scans are often collected in routine clinical computer-aided design practice, detailed internal anatomy imaging (e.g., MRI or CT) is not. We present a prototype statistical shape model (SSM) describing the transtibial amputated residual limb, generated using a sparse dataset of 33 MRI and CT scans. To describe the maximal shape variance, training scans are size-normalized to their estimated intact tibia length. A mean limb is calculated and principal component analysis used to extract the principal modes of shape variation. In an illustrative use case, the model is interrogated to predict internal bone shapes given a skin surface shape. The model attributes ~52% of shape variance to amputation height and ~17% to slender-bulbous soft tissue profile. In cross-validation, left-out shapes influenced the mean by 0.14–0.88 mm root mean square error (RMSE) surface deviation (median 0.42 mm), and left-out shapes were recreated with 1.82–5.75 mm RMSE (median 3.40 mm). Linear regression between mode scores from skin-only- and full-model SSMs allowed prediction of bone shapes from the skin with 3.56–10.9 mm RMSE (median 6.66 mm). The model showed the feasibility of predicting bone shapes from surface scans, which addresses a key barrier to implementing simulation within clinical practice, and enables more representative prosthetic biomechanics research.

This research article was awarded Open Data badge for transparent practices. See the Data Availability Statement for details.

© The Author(s), 2025. Published by Cambridge University Press. This is an Open Access article, distributed under the terms of the Creative Commons Attribution licence (http://creativecommons.org/licenses/by/4.0), which permits unrestricted re-use, distribution and reproduction, provided the original article is properly cited.

https://doi.org/10.1017/dce.2025.10019 Published online by Cambridge University Press

Impact Statement

The presented statistical shape model answers calls from the prosthetics community for residual limb shape descriptions to support prosthesis structural testing that is representative of a broader population. The SSM allows, for example, definition of worst-case residual limb sizes and shapes toward testing standards. Furthermore, the lack of internal anatomic imaging is one of the main barriers to implementing predictive simulations for prosthetic "socket" interface fitting at the point of care. Reinforced with additional data, this model may enable generation of estimated finite element analysis models for predictive prosthesis fitting, using 3D surface scan data already collected in routine clinical care. This would enable prosthetists to assess their design choices and predict a socket's fit before fabrication, important improvements to a time-consuming process which comes at high cost to healthcare providers. Finally, few researchers have access to residual limb anatomy imaging data, and there is a cost, inconvenience, and risk associated with putting the small community of eligible participants through CT or MRI scanning. The presented method allows sharing of representative synthetic residual limb shape data while protecting the data contributors' privacy, adhering to GDPR. This resource has been made available at https://github.com/abel-research/OpenLimbTT, open access, providing researchers with limb shape data for biomechanical analysis.

1. The need for statistical models to support prosthetic limb design

Over 5000 major lower limb amputations are performed every year in the United Kingdom (NHS England Secondary Care Analytical Team, 2024), and an estimated population of 55–60,000 uses prosthetics services. Prosthetic limbs may enable a return to walking and other activities associated with self-care, community engagement, education, and employment. However, the tissues in the residual limb are not initially suited to supporting the large mechanical loads transferred across the prosthesis–limb interface, which most commonly comprises a thermoplastic or composite "socket." The design and fitting of the socket are key in balancing comfort with firm, functional load transfer. The residual limb tissues' size, shape, and mechanical load tolerance vary considerably within and between individuals. Therefore, each socket must be designed with a bespoke shape and choice of materials, and components for the management of volume change and suspension (Safari and Meier, 2015). Poorly fitting and misaligned sockets are uncomfortable and can lead to sores, ulcers, and deep tissue injury (Rogers and Khatib, 2024).

An understanding of residual limb shape and tissue composition is thus crucial to designing a well-fitting socket. The socket design typically refers to a pattern of "rectifications," where the socket shape deviates strategically from that of the limb, to achieve desired load transfer through local interference at load tolerant sites, and offloading vulnerable sites. Conventionally the socket is designed manually using plaster casting by a highly experienced prosthetist. They must decide on the most appropriate design approach and identify landmarks by palpating the surface of the limb. Although general design approaches exist, there is no clear quantitative consensus between prosthetists on the exact location, shape, or relative size of the rectifications (Dickinson et al., 2021). This results in a skill-based design process that is near impossible to reproduce, and clinicians call for tools to allow more evidence-based evaluation and prediction of socket fit (Safari and Meier, 2015). Computer-aided design and manufacturing (CAD/CAM) technologies are growing in use to create socket designs through digital modification of a 3D surface scan, before carving a foam mold for socket fabrication. CAD/CAM requires the same clinician experience and skill as plaster methods, but preserves a digital design record and could permit a marked improvement to the efficacy and clinical efficiency of the design process. For example, a data-informed design process could enable prosthetists to apply lessons learned from previous design records (Lemaire and Johnson, 1996; Mbithi et al., 2025), or to accurately predict interface pressure, allowing a clear indication of fit prior to fabrication (Goh et al., 2005). However, only a small proportion of these technologies' potential is currently being exploited (Oldfrey et al., 2024).

Moving from the clinic to the research domain, related efforts to improve socket design with prediction have developed finite element analysis (FEA) methods to predict residual limb–socket interface stresses, and the resulting residual limb tissue strains, enabling parametric socket design analysis (Dickinson et al., 2017). However, building an FE model of the residuum socket system requires patient-specific

https://doi.org/10.1017/dce.2025.10019 Published online by Cambridge University Press

information, primarily the residual limb tissues' shape, tissue composition, material properties, and the dynamic mechanical loading. Although CAD/CAM methods provide accurate external shape data, volumetric imaging data are required to capture the internal anatomic details generally included in FE models (Ramasamy et al., 2018; Steer et al., 2021). Internal tissues are conventionally imaged in 3D using MRI or CT scans, however, these are not conducted as part of routine prosthetic care due to cost, time, and CT's radiation dose. The same barriers exist in prosthetics biomechanics research, where shape data availability is restricted, and often limited to the more routinely collected external surface scans.

Statistical shape models (SSM) (Stegmann and Gomez, 2002) may offer solutions to the barriers against access to medical imaging data for FEA and prosthetic socket design analysis. When applied to medical imaging, SSMs allow a stochastic description of the anatomy within a given population by extracting patterns of shape variance in a sample of training data. This analysis enables the dimensionality of the population's characteristics to be reduced to a limited number of important modes of variation (Audenaert et al., 2019). If an SSM is made using an appropriate quantity and diversity of training data, a variety of use cases become available. SSMs are frequently employed in orthopedics and biomechanics to classify anatomy (Worsley et al., 2015) or disease (Ambellan et al., 2019), to identify potential risk factors contributing to fractures (Grassi et al., 2021), and to predict missing data from partial information (Woods et al., 2017) such as estimating 3D models from 2D x-ray images (Blanc et al., 2012). A limited number of studies have also predicted skeletal geometry from exterior surface shapes using this approach (Keller et al., 2022; Shetty et al., 2023). A statistical residual limb shape model would potentially address the abovementioned data limitations, offering a means to support biomechanical simulation and prosthetic device design where there is a lack of complete anatomic data (Saxby et al., 2020), such as predicting internal anatomy given an exterior surface scan. Prior applications in lower limb prosthetics have used SSM to study variations in proximal tibia shape (Hafner et al., 2000), and combined the method with linear discriminant analysis for objective residual limb shape classification into clinically relevant groups according to shape (Worsley et al., 2015). Costa et al. used SSM to capture variations in socket shape (Costa et al., 2021) and hypothesized that such a tool could provide on-demand socket design insights, whereas Dickinson et al. (2021) performed statistical shape analysis on both residual limbs and their corresponding sockets, identifying key trends in the choice of design approaches used by expert prosthetists. Steer et al. (2020) proposed a method of predictive prosthetic socket design by creating multiple FE models of transtibial residual limbs using SSM to offer a solution to the model generation workload, computational expense, and training barriers to performing conventional FEA in a clinical setting. However, these studies have considered only the external shape of the residual limb from CAD/CAM 3D scan data or approximated the internal geometry by scaling the bone models from a single MRI dataset. Most recently, the American Orthotic and Prosthetic Association (AOPA) Socket Guidance Work group has identified a need for descriptions of the shape and composition of residual limbs in the generation of mock limb models to aid structural testing of prosthetic sockets (Gariboldi et al., 2023). Therefore, the research and clinical communities have communicated a need, and a variety of use cases, for accessible data on the external and internal anatomy of the amputated residual limb, a gap which this article aims to address.

This study therefore presents a first statistical shape model of the transtibial residual limb from volume medical imaging data (i.e., MRI and CT) that includes both the exterior surface and the internal bony anatomy, and assesses its ability to allow prediction of internal bony anatomy from the exterior surface alone. This comprises methodological novelty relevant to sparse, partial datasets arising from the compounded effects of both anatomical and surgical variation which affect amputation and prosthetics.

2. Creating a population model from sparse, incomplete anatomic data

2.1. Subject data and ethics

Secondary data analysis ethical approval was granted by the University of Southampton's Ethics Committee (ERGO II 65748A2). Subject data consisted of MRI or CT scans of 43 people with residual

https://doi.org/10.1017/dce.2025.10019 Published online by Cambridge University Press

Table 1. *Details of the included individuals*

Age, years; median (range)	54 (25–81)
Time since amputation, years; median (range)	4.1 (1–35)[a]
Sex	4F 29M
Amputation side	18 Left, 15 right[b]
Amputation cause	9 Trauma 3 Vascular disease 2 Chronic pain 19 Not recorded[c]
Ethnicity	12 White European/US 9 Latino 5 Native American 1 African American 6 Not recorded
Height, m; median (range)	1.76 (1.53–1.89)
BMI, kg/m^2; median (range)	27.5 (16.7–53.0)[a]

Note. Four of the obtained datasets were excluded after building a preliminary SSM and their details are left out of this table.
[a]For NMDID datasets (Edgar et al., 2020; Finco et al., 2023), weight and time since amputation were not provided.
[b]Two participants had bilateral amputations and only their right residual limb was used in the model.
[c]NMDID did not report reasons for amputation, however, of these 18 individuals three had a listed Type I diabetes diagnosis, and 10 Type II diabetes, so the vascular disease cause is likely to be an under-estimate.

limbs from transtibial amputations using five different sources, collected in previously published research, and/or provided to the authors under data sharing agreements (Steer, 2019; Bramley, 2020; Edgar et al., 2020; Mendis, 2021; Ding et al., 2023; Finco et al., 2023). The participants covered a range of amputation causes, age, and time since amputation (Table 1). Six scans were excluded due to failing to satisfy at least one of the following inclusion criteria, such that the model would describe a cohesive population and consistent anatomical features:

- Amputation through the tibial diaphysis, that is, excluding e.g. Symes amputation.
- The limb and scan must have the typical residual skeletal anatomy for a transtibial amputation, that is, distal femur, patella, proximal tibia, and proximal fibula should be present.
- Standard surgical amputation technique must have been used for the amputation, without additional reconstruction, that is, excluding bone-bridging or capping or implants for prosthesis suspension.

Four more scans were excluded from the dataset after producing a preliminary model which identified very substantial imaging artefacts, as explained next.

2.2. Residual limb processing

2.2.1. Mesh generation and alignment

The raw MRI and CT DICOM image sets representing transverse slices were segmented to provide corresponding surface meshes of the skin and residual tibia, residual fibula, patella, and distal femur bones, in .stl format (ScanIP Version 2018.12; Synopsys, Inc., Mountain View, USA).

The MRI and CT scans were taken with the patient supine with the posterior aspect of their residual limb supported. While this gives an approximately standardized pose, the orientation still varied between limbs. By aligning the training datasets, variations in relative position and orientation can be removed such that the SSM is able to describe more detailed anatomic shape variation. Due to differences in remaining anatomy and intersubject variation in knee joint alignment, the alignment of the proximal residual tibias was prioritized.

https://doi.org/10.1017/dce.2025.10019 Published online by Cambridge University Press

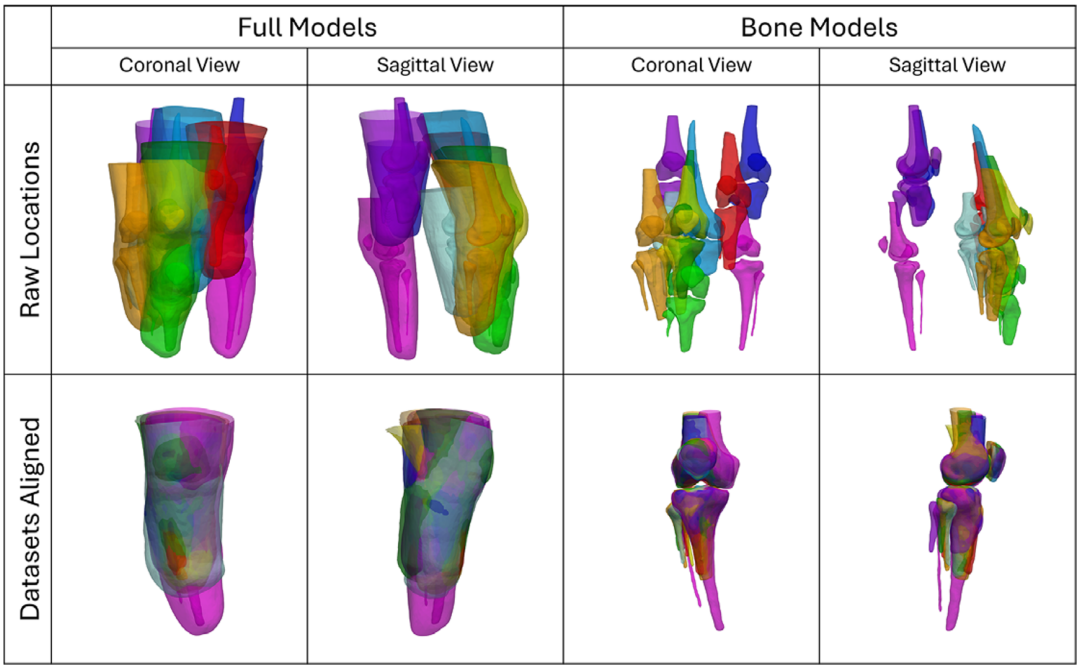


Figure 1. *Coronal and sagittal views of the first 10 subjects' training data (full and bones only) meshes before (top) and after the alignment and trimming were performed (bottom).*

First, each limb was aligned with respect to a global coordinate system (CS) defined by the International Society of Biomechanics convention (*xz* plane = transverse, *yz* = coronal, *xy* = sagittal) (Wu et al., 2005) using the ampscan open-source shape analysis toolbox (Steer et al., 2020). The alignment procedure was as follows (Figure 1):

- left-sided shapes were mirrored so that all subjects were the same side,
- shapes were then translated so that their tibia mesh vertex centroids lay at the origin,
- shapes were rotated to align their tibia mesh principal axes of inertia, estimated using PCA, with the global coordinate axes,
- finally, datasets were rotated about the vertical axis so that the posterior extents of the knee condyles lay along a medial–lateral axis.

Second, an iterative closest point (ICP) rigid registration algorithm was used to adjust each dataset's alignment with respect to the tibia, to maximize intersubject alignment, followed where necessary with small manual adjustments by an experienced human observer. After alignment, a trim was applied in the transverse plane at a level one patella height above the most proximal extent of the patella, to include a consistent degree of geometry above the knee relevant to supracondylar socket designs.

2.2.2. Size normalization

SSMs are often created using size-normalized training data, to separate size and shape variance. However, due to variations arising from surgery, each of the training shapes' residual limb length represents a different proportion of the intact limb, so a simple scaling factor is not sufficient to ensure the mapping of corresponding anatomical features (Lam et al., 2016). For example, a taller individual with a relatively high amputation may have a longer residual limb than a shorter individual with much more intact anatomy. Therefore, this study size normalized the training shapes to the full tibia length, T as the unit

https://doi.org/10.1017/dce.2025.10019 Published online by Cambridge University Press

size. This was taken from the contralateral limb images where available, or estimated from the individual's height, H (mm), and their age, A (years), using a regression formula (Eq. 1) (Trotter and Gleser, 1952):

$$T_{male} = \frac{H - 786.2 + 0.6\alpha}{2.52}, \quad T_{female} = \frac{H - 615.3 + 0.6\alpha}{2.90} \tag{1}$$

where α is defined in

$$\alpha = \begin{cases} 0 \, if \; A \leq 30 \\ (A - 30) \, if \; A > 30. \end{cases} \tag{2}$$

Following size normalization a visual check of alignment was made

2.2.3. Registration

Mesh registration is necessary for point-to-point comparison between each of the SSM's training shapes so that they are represented using a corresponding set of vertices, allowing their shape variance to be extracted. A "baseline" shape was chosen and each of its mesh bodies mapped onto the surface of the corresponding "target" data subject bodies using Amberg and Romdhani's (Amberg et al., 2007) nonrigid ICP algorithm in the trimesh package (Dawson-Haggerty, 2019). This algorithm was selected as it is less sensitive to outliers and missing data than conventional elastic matching methods. This deforms the baseline toward the target incrementally, permitting accurate registration of anatomy present in both datasets, and appropriately distributed mesh vertices in cases where the anatomy in the baseline mesh is not present on the target dataset. Figure 2 depicts an example of the key steps applied to one of the skin meshes, including over scaling the baseline to the target to ensure registration of the model's open proximal boundary.

2.3. Statistical analysis

Principal component analysis (PCA) is considered the standard approach used for creating statistical shape models (Stegmann and Gomez, 2002). PCA objectively identifies patterns of shape variance (modes) in a set of training data. This analysis enables the dimensionality of the population's characteristics to be reduced by selecting a limited number of important modes of variation, that is, principal components (PCs) (Audenaert et al., 2019). PCA describes how each training dataset compares to the population mean shape, described by a "score" in each mode of variation. Two statistical limb shape models were produced by PCA, representing the skin and bone surfaces ("full model," μ) and the skin surface only ("skin model," μ^s), using the scikit-learn toolbox (Abraham et al., 2014). The procedure was an extension to method which was previously reported for analyzing the residual limb's external shape (Dickinson et al., 2021).

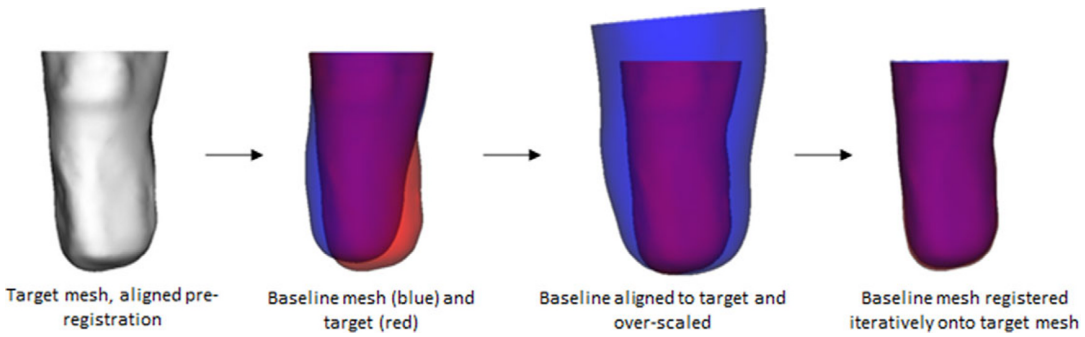


Figure 2. *The main steps in registration (original, aligned, scaled, and registered meshes, from left to right).*

https://doi.org/10.1017/dce.2025.10019 Published online by Cambridge University Press

First, the mesh vertices $\boldsymbol{x}_i$ for each i of the n training individuals were each represented as a column vector, Eq. (3), where m represents the number of vertices in the baseline mesh and x, y, and z; are the vertex coordinates,

$$\boldsymbol{x}_i = [x_1, y_1, z_1, \ldots, x_m, y_m, z_m]^T. \tag{3}$$

A column vector representing the mean limb shape was then calculated using, Eq. (4),

$$\bar{\boldsymbol{x}} = \frac{1}{n}\sum_{i=1}^{n} \boldsymbol{x}_i, \tag{4}$$

where n represents the number of limbs in the training dataset, giving Eq. (5),

$$\bar{\boldsymbol{x}} = [\bar{x}_1, \bar{y}_1, \bar{z}_1, \ldots, \bar{x}_m, \bar{y}_m, \bar{z}_m]^T; \tag{5}$$

and the meshes were mean centered according to Eq. (6),

$$\boldsymbol{x}_{i\,mc} = \boldsymbol{x}_i - \bar{\boldsymbol{x}}. \tag{6}$$

PCA by singular value decomposition (SVD) was then performed. This enabled each limb shape to be described by Eq. (7), where $\boldsymbol{Aj}$ represents the eigenvectors corresponding to the each of the c modes of population shape variation,

$$\boldsymbol{x}_i = \bar{\boldsymbol{x}} + \sum_{j=1}^{c} \boldsymbol{Aj}\boldsymbol{\lambda j}_i. \tag{7}$$

and $\boldsymbol{\lambda j}$ is a vector of weighting coefficients or "mode scores," associated with the eigenvectors to describe each training dataset shape's deviation from mean, with $\boldsymbol{\lambda j}$ being represented by Eq. (8),

$$\boldsymbol{\lambda j} = [\lambda j_1, \ldots, \lambda j_n]. \tag{8}$$

The approximated 95% range of population variation was plotted by generating synthetic shapes (η) with weighting coefficients defined using the training dataset's 2.5th and 97.5th percentile mode scores for each mode j in turn using Eqs. (9 and 10), allowing visual interpretation of the shape variance contained within the mode,

$$\boldsymbol{\eta}_{j0.025} = \boldsymbol{A}\boldsymbol{\lambda j}_{.025} + \bar{\boldsymbol{x}}, \tag{9}$$

$$\boldsymbol{\eta}_{j0.975} = \boldsymbol{A}\boldsymbol{\lambda j}_{.975} + \bar{\boldsymbol{x}}. \tag{10}$$

During model generation, all training shapes' mode scores were inspected. Four shapes were observed to have very distorted soft tissues associated with positioning in the MRI or CT scanner, identified by outlying influence in both extremes of leave-one-out cross-validation tests, so they were set aside leaving a training dataset of 33.

2.4. Statistical shape model performance and validity testing

2.4.1. Compactness: how many modes of variability does the model require?

As PCA is a dimensionality reduction technique, the compactness describes the ability of the SSM to represent the population variation with a minimal subset of modes (Pearson, 1901). Compactness was assessed by reconstructing each training individual (i) with progressively increasing number of modes (j) and calculating the root mean square error (RMSE or ε_j) of vertex surface deviation between the reconstruction ($\widetilde{\boldsymbol{x}}_{ij}$) and the original data ($\boldsymbol{x}_i$), such that Eq. (11) represents each reconstruction

https://doi.org/10.1017/dce.2025.10019 Published online by Cambridge University Press

$$\begin{aligned}\tilde{\boldsymbol{x}}_{i_0} &= \overline{\boldsymbol{x}} \\ \tilde{x}_{i_1} &= \overline{\boldsymbol{x}} + A_1\lambda_{1_i} \\ \tilde{\boldsymbol{x}}_{i_2} &= \overline{\boldsymbol{x}} + A_1\lambda_{1_i} + A_2\lambda \\ &\vdots \\ \tilde{\boldsymbol{x}}_{i_c} &= \overline{\boldsymbol{x}} + A_1\lambda_{1_i} + A_2\lambda_{2_i}\cdots + Ac\lambda c_i\end{aligned} \tag{11}$$

and Eq. (12) represents the error

$$\begin{aligned}\varepsilon_{n_0} &= \boldsymbol{x}_i - \tilde{\boldsymbol{x}}_{i_0} \\ \varepsilon_{n_1} &= \boldsymbol{x}_i - \tilde{\boldsymbol{x}}_{i_1} \\ &\vdots \\ \varepsilon_{n_c} &= \boldsymbol{x}_i - \tilde{\boldsymbol{x}}_{i_c}\end{aligned} \tag{12}$$

2.4.2. Generality by cross-validation: how much does leaving training shapes out affect the mean and extreme mode shapes?

Generality assesses whether a model can accurately describe similar shapes that have not been included in the training set, and the effect of noise in the training data (Lam et al., 2016). Generality is commonly determined using leave-one-out (LOO) cross-validation testing allowing identification of the model's accuracy given the available training data, or whether that available training dataset size is sufficient for some acceptable error level. This is measured by assessing the influence of leaving out each shape (i) on the mean and extreme mode shapes. Each shape was left out, one at a time, and a new $\bar{\boldsymbol{x}}_i$ and $\boldsymbol{\mu}_i$ were generated. The influence of each shape can be evaluated by calculating root mean squared errors (RMSEs) between mean shapes and mode extremes generated from the full SSM ($\boldsymbol{\mu}_i$) and SSMs with each shape left out.

2.4.3. Generality by recreation: how accurately can the model describe left-out shapes?

Generality was further assessed by evaluating how well the SSM can describe a new data set not used in its creation by using each LOO-SSM model from the cross-validation test to recreate the left-out shape. The left-out shape's mode scores λ ($m \times 1$ column vector) were estimated by solving the least squares matrix problem. Conventionally this takes the form $\boldsymbol{A}\boldsymbol{x} = \boldsymbol{b}$, though we are prioritizing nomenclature convention used in SSM studies, in Eq. (13),

$$\boldsymbol{A}\boldsymbol{\lambda} = \boldsymbol{x}, \tag{13}$$

where $\boldsymbol{A}$ is the $m \times c$ matrix representing the principal components (Aj) and $\boldsymbol{x}$ is the $m \times 1$ column vector representing the left-out shape's vertex coordinates, see Eq. (2). Note c, the number of modes (PCs), will be one less in the LOO-SSMs than in the full SSM because the number of modes that can be determined is equal to $n - 1$. As $\boldsymbol{A}$ is not a square matrix it is not invertible, therefore, the Moore–Penrose pseudoinverse was computed to solve Eq. (13) (*Generalized Inverses*, 2003), using NumPy's linear algebra submodule.

2.5. Example use case: Shape prediction from partial data

A common use of SSMs is prediction of a shape given only partial data. An application of the present model might be to predict the internal geometry from the external shape. Two methods were compared.

First, a similar pseudoinverse method to that used earlier for model recreation was tested. For this purpose, a consistent partial shape, the skin, and consistent missing data, the bones, were used. This means that point-to-point correspondence between the partial shape and the SSM was known. This method is also known as Gappy POD (proper orthogonal decomposition) (Bui-Thanh et al., 2004). In place of Eq. (13), Eq. (14) provides,

$$\boldsymbol{A}^s\boldsymbol{\lambda} = \boldsymbol{x}^s, \tag{14}$$

where $\boldsymbol{A}^s$ is the subset of $\boldsymbol{A}$ that only contains the first s rows that act on the skin nodes, and $\boldsymbol{x}^s$ is the SSM skin mesh registered to the partial shape. Employing the earlier method, mode scores can be estimated and then used with the complete principal components to predict a complete shape.

https://doi.org/10.1017/dce.2025.10019 Published online by Cambridge University Press

An alternative method employing linear regression was also tested (Figure 3). Training dataset mode scores calculated from each leave-one-out skin only model were collected alongside the corresponding mode scores from each leave-one-out full model, and a linear regression between each pair of mode scores was formulated using scikit-learn (Abraham et al., 2014), such that the full mode scores were the dependent variable. The recreation method, provided in "Generality by recreation," was used upon the skin-only leave-one-out model to estimate mode scores and thus recreate each left out shape's skin.

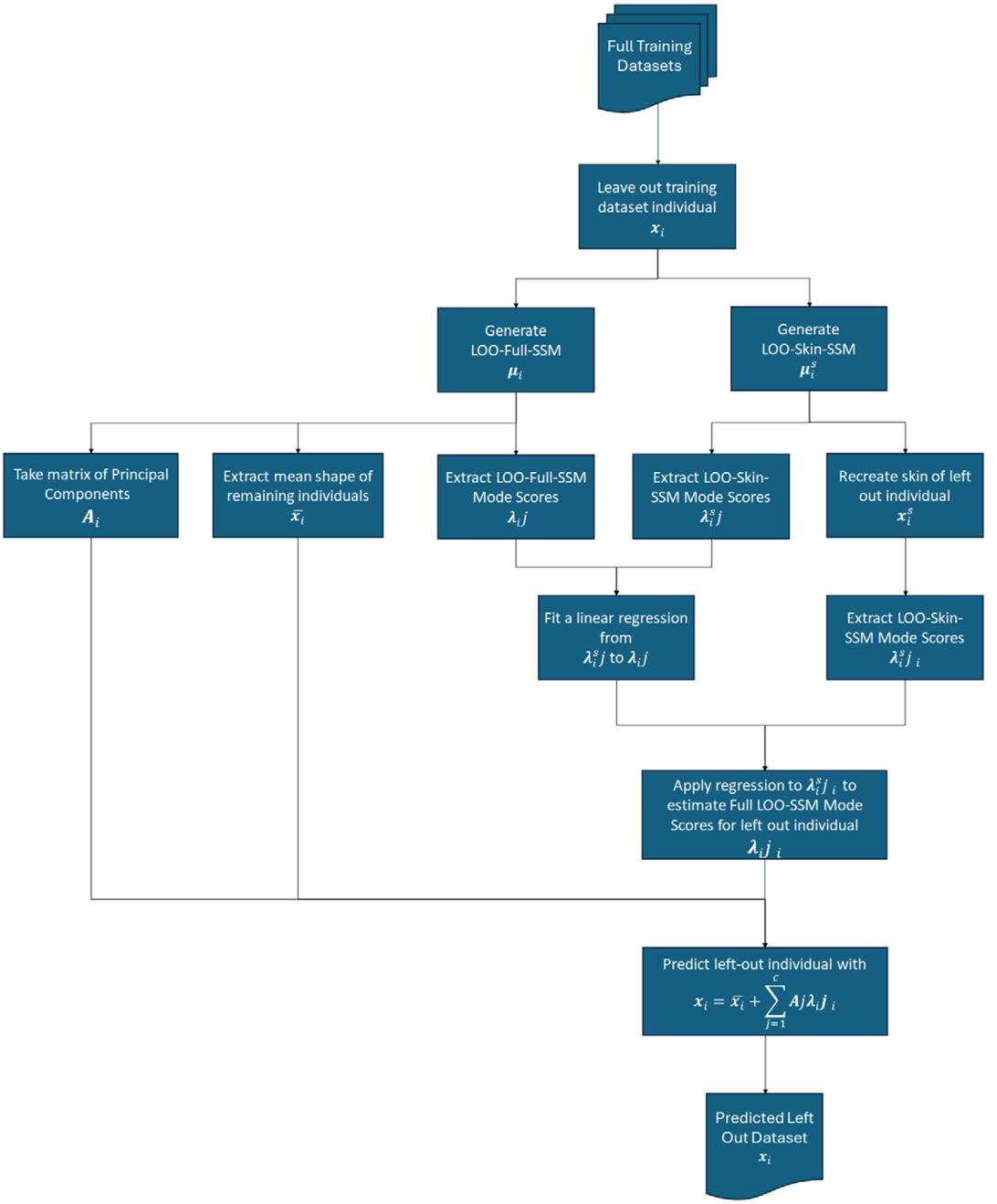


Figure 3. *Flowchart of steps in linear regression prediction method.*

https://doi.org/10.1017/dce.2025.10019 Published online by Cambridge University Press

The corresponding leave-one-out regression was then fitted to the skin-only mode score estimates to predict mode score values for the full model's description of the left-out shape. Using these predicted scores, a predicted shape was generated using Eq. (8) and plotted. This was then aligned with the actual left-out shape and the RMSE calculated. In addition to mean centering and scaling, the PCA used scikit-learn's "whitened" components scores to minimize linear correlation across features.

The prediction accuracy was calculated with both methods as the RMSE between the actual and predicted shapes for (i) the bones, (ii) the skin, and (iii) the whole limb. The RMSE was calculated with the normalized data and expressed in mm by rescaling back to the actual size. Differences in accuracy between the prediction methods were assessed for statistical significance with a nonparametric Wilcoxon signed rank test, for paired data.

3. Statistical shape model, validation, and use case for internal anatomy prediction

3.1. Modes of variation

The participants' known or estimated full tibia lengths indicated that the training shapes represented a median 36% of the intact anatomy. The proportionally shortest and longest limbs preserved 18% and 60% of the intact tibia length, respectively (Appendix 1). After size normalization, the average locations of vertices in the aligned, registered training shape meshes were calculated to produce the population mean shape (Figure 4). The PCA calculation provides the proportion of population variance attributed to each mode of shape variation (Figure 5) and indicates that 69% of the population variance was contained within the first 2 modes and 95% within 10 modes, implying that these are most important for describing or classifying gross shape.

The shapes of these nine primary independent modes of limb variation were plotted to permit inspection of the variance they represent (Figure 6). The variations predominantly manifested as amputation height in Mode 1 which encompasses 52.2% of the population variance, and slenderness/soft tissue bulk in Mode 2, including 16.7% of the variance. As discussed later, these external shape variations are consistent with previous SSMs. However, this model provides first quantitative insights into how the internal and external anatomic shape variation is related. For example, Mode 3 (8.2% of variance) represents the relative scale of the bones within the soft tissue, and along with modes 5 (3.1%) and 6 (2.6%) includes varying distal soft tissue coverage over the distal tibia bony prominence, a notable site of particular soft tissue vulnerability and relevance in socket design. These modes illustrate how a relatively shorter residual bone allows the posterior soft tissue more freedom to deform posteriorly and medially. The model also shows variance which might be associated with scanning; Mode 4, 7.2% of the population variance, describes knee flexion, and Modes 5 (3.1) and 8 (1.3%) describe posterior and

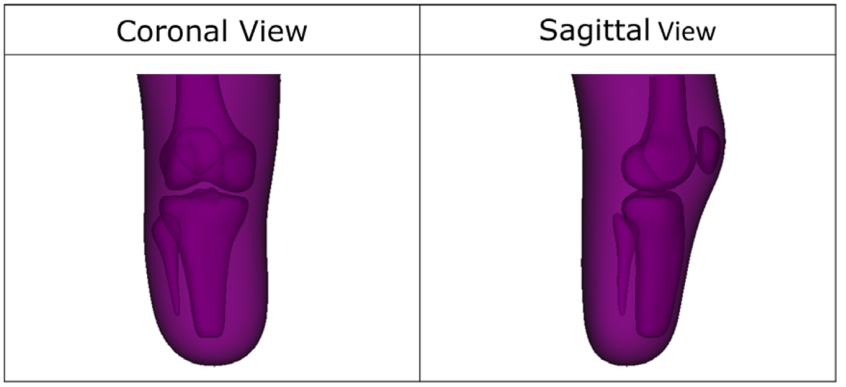


Figure 4. *Mean of residual limb training shapes.*

https://doi.org/10.1017/dce.2025.10019 Published online by Cambridge University Press

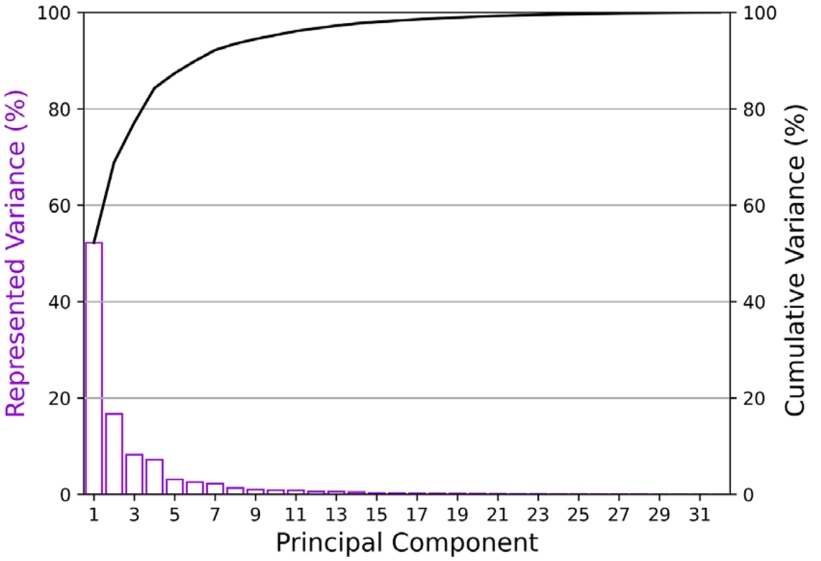


Figure 5. *Individual and cumulative variance represented by each mode of the full statistical shape model.*

medial variation in soft tissue distribution which might be associated with soft tissue deformation under the body's self-weight and contact with the scanner bed, respectively, in the calf and thigh.

3.2. Validity tests

Compactness testing (Figure 7) demonstrated that by employing the initial 10 modes which encompass 95% of the variance, all training shapes could be reconstructed with an RMSE below 5 mm. In context, the training shapes were a median of 14 mm RMSE (range 4–30 mm) from the mean shape, indicated by their reconstruction without using any SSM modes. In cross-validation testing (Table 2), the mean and 2.5th and 97.5th percentile extreme shapes in each mode were generated for each of the LOO-SSMs and compared to the corresponding shapes obtained from the full SSM. Leaving out training shapes had little influence on the mean, at 0.14–0.88 mm RMSE surface deviation (median 0.42 mm). The RMSEs associated with leaving out individual shapes were also small for the extreme shapes in Modes 1 and 2 (medians of 0.36–0.70 mm, and interquartile ranges [IQR] of 0.66–1.06 mm, respectively), however, given the limited training dataset size, individual shapes could disproportionately affect single modes. This is evidenced by two outliers in Mode 1, represented by training datasets 10 and 20, which were considerably longer than the rest (Table A1); leaving each of them out influenced the long-length extreme shape by 8.29 and 8.97 mm, respectively, but did not substantially influence the short length extreme.

3.3. Prediction of bones from residual limb surface

The model's ability to predict each residual limb's bony anatomy from its external surface was evaluated and compared to the model recreation (Figure 8). Four shapes are presented to illustrate relatively good and poor examples of the model's predictive capabilities. Participant IDs 1 and 2 (Figure 8, rows 1 and 2) are both near the population mean in Mode 1. Both methods predicted the soft tissue shape well, and displayed some inaccuracies, particularly with respect to predicting individual bony anatomy characteristics. For example, ID1 has a relatively short residual fibula, and ID2 has a quite lateralized fibula and femur. The PI method showed higher error in predicting soft tissue coverage over notable bony prominences such as the fibula head and distal tibia, which is potentially problematic for its use in socket design or analysis. The linear regression (LR) method produced more accurate bone shapes and slightly lower error in all the locations listed earlier. Subject ID8 is included as an example which was predicted

https://doi.org/10.1017/dce.2025.10019 Published online by Cambridge University Press

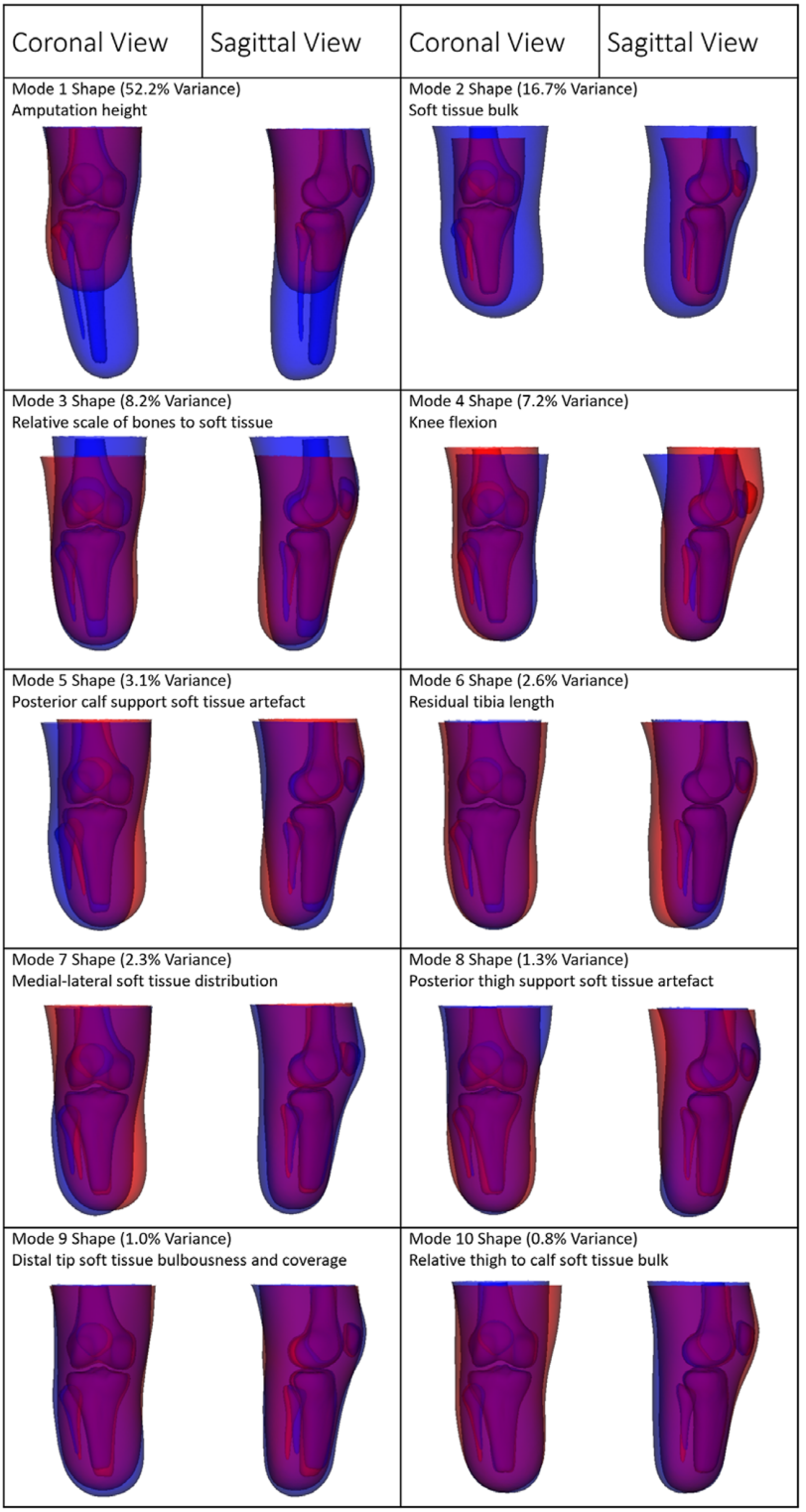


Figure 6. *SSM mode shapes as described by 2.5th (blue) to 97.5th percentile (red) estimated variance range from in the training dataset. These permit the principal modes of residual limb shape variance to be inspected.*

https://doi.org/10.1017/dce.2025.10019 Published online by Cambridge University Press

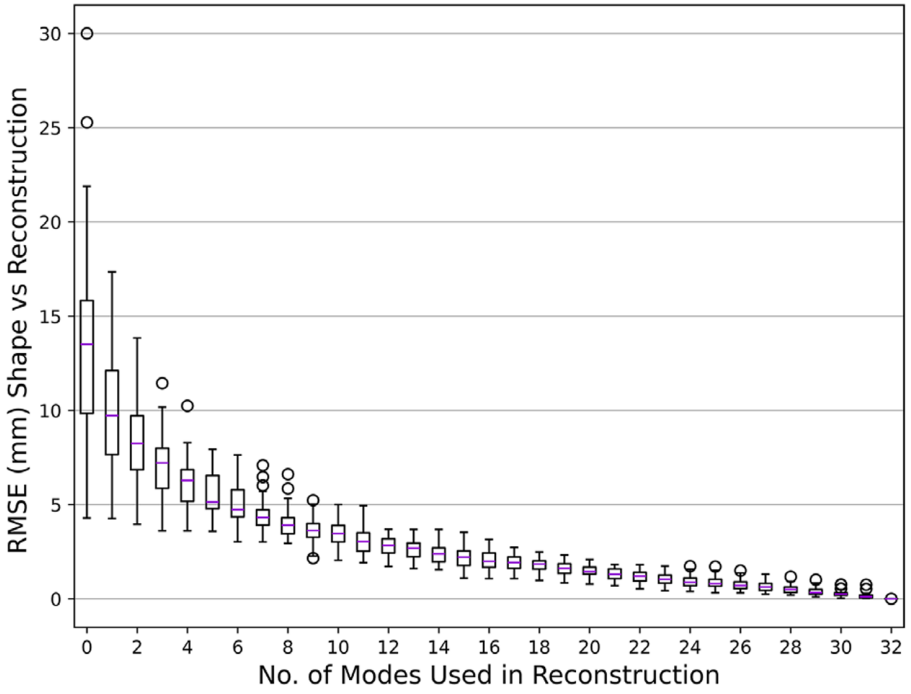


Figure 7. *Compactness: range of RMSE between each subject's actual shape and its reconstruction from the SSM using a reduced number of modes. Normalized data rescaled back to actual size for expression in mm.*

Table 2. *Variation of the leave-one-out statistical shape model (LOO-SSM) for mean and first two mode shapes compared to the full SSM*

Shape	Median RMSE (mm)	IQR RMSE (mm)	Min RMSE (mm)	Max RMSE (mm)
Mean	0.42	0.26	0.14	0.88
Mode 1: 97.5% (long)	0.70	0.74	0.09	8.97
Mode 1: 2.5% (short)	0.36	0.66	0.03	1.99
Mode 2: 97.5% (bulbous)	0.61	1.06	0.06	3.92
Mode 2: 2.5% (slender)	0.61	0.84	0.15	2.38

Note. Normalized data rescaled back to actual size for expression in mm. RMSE: root mean squared error; IQR: interquartile range.

poorly by both methods (Figure 8, row 3) as it features unique bony characteristics which were far from the population mean and not indicated by the external soft tissue shape: the very short fibula and the relatively short tibia compared to the full limb length, represented as high tissue thickness at the limb's distal end. The other main weakness in prediction is demonstrated by Subject 10 (Figure 8, row 4) who has a considerably longer residuum (60% of intact tibia) compared to the rest of the training dataset. This is difficult to predict because it features anatomy not present in the remainder of the training data. Relative to the recreation, the PI method performs particularly well especially in the prediction of distal soft tissue coverage, however, both methods are limited by the model's inability to describe the longer limb shape and very slender distal bony anatomy.

https://doi.org/10.1017/dce.2025.10019 Published online by Cambridge University Press

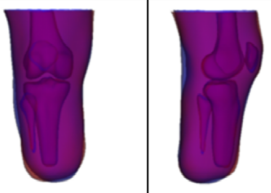
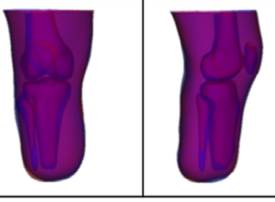
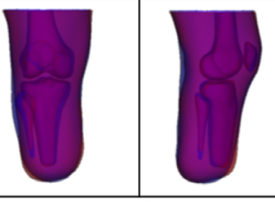
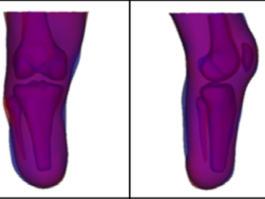
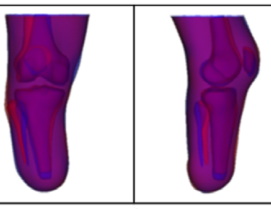
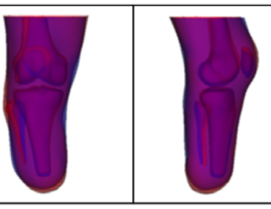
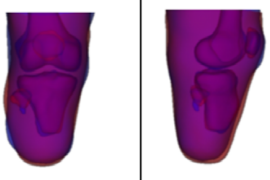
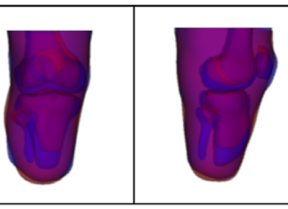
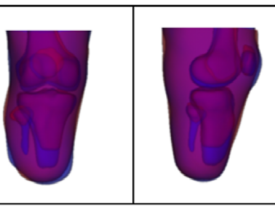
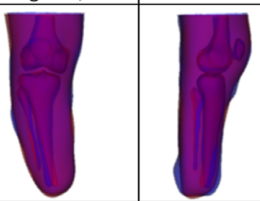
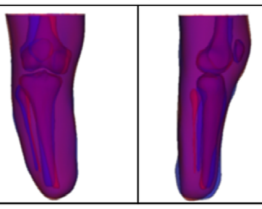
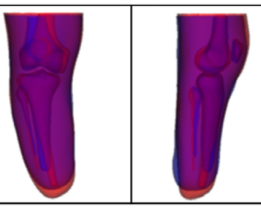
	Recreated Shape (blue) vs. Original Shape (red)		PI Prediction of Shape (blue) vs. Original Shape (red)		LR Prediction of Shape (blue) vs. Original Shape (red)	
	Coronal	Sagittal	Coronal	Sagittal	Coronal	Sagittal
ID 1, 35% Tibia						
	RMSE (all), mm	2.30	3.87		2.85	
	RMSE (bone), mm	2.24	6.00		3.56	
	Coverage Err, mm	2.13	-6.89		1.29	
ID 2, 39 % Tibia						
	RMSE (all), mm	2.83	4.87		4.70	
	RMSE (bone), mm	2.68	7.72		5.74	
	Coverage Err, mm	-2.33	-12.00		-4.73	
ID 8, 23% Tibia						
	RMSE (all), mm	3.71	6.92		6.10	
	RMSE (bone), mm	3.42	10.71		8.00	
	Coverage Err, mm	-5.44	-21.61		-23.66	
ID 10, 60% Tibia						
	RMSE (all), mm	4.01	5.17		7.77	
	RMSE (bone), mm	5.01	8.01		10.49	
	Coverage Err, mm	-5.93	3.65		24.57	

Figure 8. *Four example subjects' original (red) compared to recreated (blue) shapes, and shapes predicted using pseudoinverse (PI) and linear regression (LR) methods alongside error measurements (mm). Normalized data rescaled to actual size for expression in mm; % in row headers refers to proportion of intact tibia remaining.*

Quantifying the overall errors for predicting the full shapes (Figure 9), both the linear regression and pseduoinverse methods give a similar spread of values (LR: median 4.97 mm, IQR 1.94 mm; PI: median 5.42 mm, IQR 1.50 mm), but the LR method outperforms the PI method overall ($p = .012$, effect size = −0.4). This trend became stronger considering the bone prediction alone, approaching the RMSE values for recreation (LR: median 6.66 mm, IQR 2.60 mm; PI: median 8.58 mm, IQR 2.84 mm; $p < .001$, effect size = −0.8). Since recreation shows the model's accuracy in describing the dataset given full

https://doi.org/10.1017/dce.2025.10019 Published online by Cambridge University Press

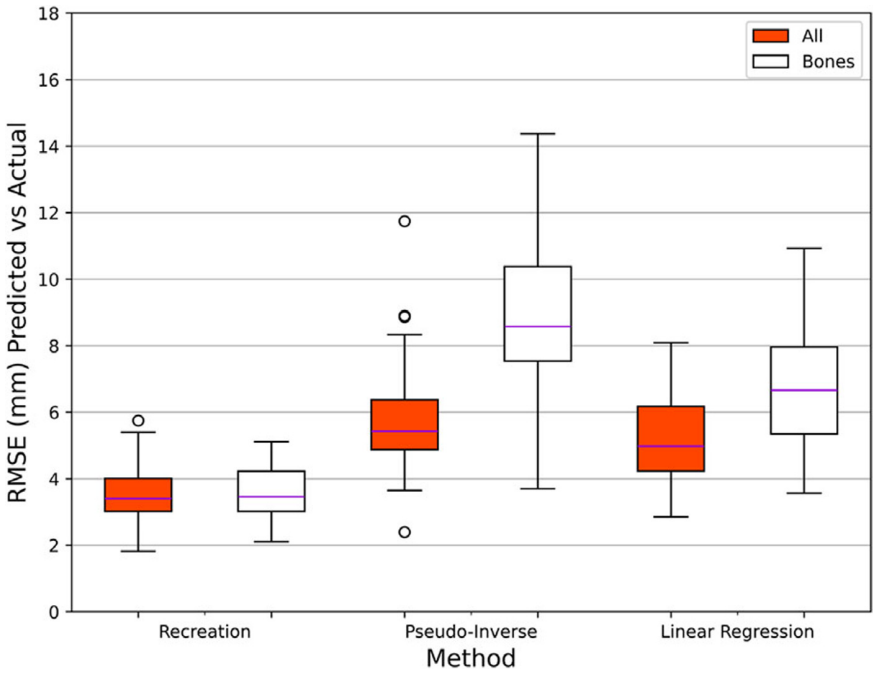


Figure 9. *RMSE of the recreated and predicted shapes compared to the actual shape. Normalized data rescaled back to actual size for expression in mm.*

information, it can be considered as the lower achievable bound for prediction error values (all: median 3.40 mm, IQR 0.99 mm; bones: median 3.46 mm, IQR 1.21 mm). Similarly, looking at the distal tissue thickness (Figure 10), LR predictions fall closer to the actual values than the PI predictions on average, but this did not reach significance ($p = 0.272$, effect size = 0.2).

4. Discussion

4.1. Observations from the SSM and corroboration

The presented residual limb SSM offers novel insights into internal anatomic variation and how it associates with surface anatomy. While the absence of comparable models means this may not be corroborated fully, it can be compared to existing models that only considered the external limb surface. The new model showed similar overall external shape variance to a residual limb surface SSM previously published by this group (Dickinson et al., 2021), in which the dominant shape variance was overall size and soft tissue bulk in Modes 1 and 2, respectively. These dimensions are key to the selection of appropriate socket design strategies. The previous, surface model's first mode contains variations in residuum size overall and length arising from amputation height, whereas the new model distinguished more clearly between these different sources of variance, especially on the sagittal view (Figure 6, Mode 1), and this advantage may arise from having size normalized the training data. Shape reconstruction errors were similar to the previously published study's residual limb external SSM for the a training dataset size of 33, and that study indicated that approximately 40 training datasets brought the error below 1 mm. This is presented as an acceptable target error level because it matches typical consistency measures in socket design (Convery et al., 2003) and residual limb shape capture by plaster casting or 3D scanning (Dickinson et al., 2022).

Comparison between the present and previous models also reveals interesting observations with regard to the diversity of the training data. The previous model included a mode shape describing coronal plane

https://doi.org/10.1017/dce.2025.10019 Published online by Cambridge University Press

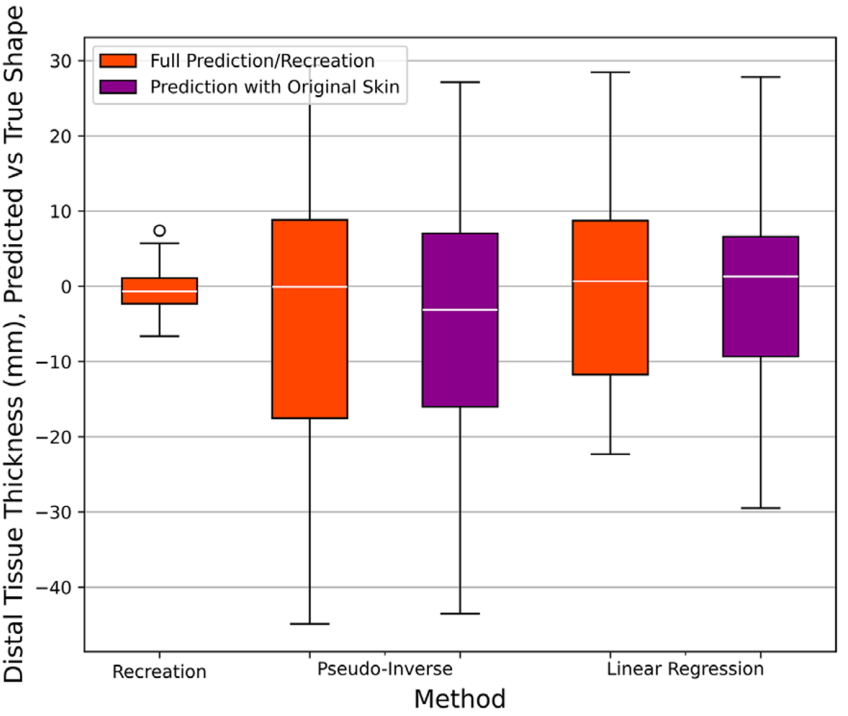


Figure 10. *Range of distal tissue thickness error (measured as most distal point of the tibia to most distal point of the skin compared to the original shape) for the recreated and predicted shapes. Normalized data rescaled back to actual size for expression in mm.*

distal bulbousness which correlated with time since amputation (Dickinson et al., 2021) and was attributed to edema which occurs commonly after amputation surgery. This often subsides in the following months, and can delay socket fitting. Such variance was not observed in this study's model, likely because all the training data came from people with at least 1-year established amputations, unlike the previous study which included some people who were very soon after amputation. Instead, the latter modes in this study's model describe internal geometry variance which could not be observed in previously published residual limb or socket SSMs. For example, variance in patella position was observed in several of the first 10 modes (Figure 6) as the training data prioritized aligning the tibia, and this will have relevance to socket design with regard to the shape of the proximal brim. Similarly, Modes 2, 4, 5, and some subsequent modes (Figure 6) show positional and length variation of the fibulae compared to the tibiae, and variation in distal soft tissue coverage. Both of these factors have an important influence on socket design to avoid loading vulnerable tissues over these potential bony prominences, which demonstrates the practical value of the novel model. Errors in tibia shape description were similar to those reported in a similar, small sample-sized, tibia-only SSM, but greatest in tibia length prediction which was outside the scope of that study (Hafner et al., 2000). With regard to the stated example use case of predicting bony anatomy from surface scans, this model demonstrated similar predictive accuracy to previous models which attempted to predict the whole skeleton given full body external shape geometry, at 3.6 mm RMSE (Shetty et al., 2023), and typical bony prominence landmark positional errors of 5–15 mm (Keller et al., 2022). Accuracy may be increased by expanding the model's training dataset, but because bony anatomy is not linked simply to limb surface shape, alternative probabilistic methods may be required to provide further improvements. An acceptable level of prediction error for bone shape is more difficult to define, with regard to the model's use in support of prosthetic socket design. Regions of low soft tissue coverage thickness over bony prominences might typically be of particular concern,

https://doi.org/10.1017/dce.2025.10019 Published online by Cambridge University Press

however, their influence in this use case is limited since socket design methods intentionally avoid loading these vulnerable sites. However, in a clinical context, the model's soft tissue thickness predictive capability could be improved using, for example, a small number of discrete linear ultrasound measurements.

This SSM also identifies some variance associated with the scanning position of the limb. Mode 4 contained variation in knee flexion pose, and other modes, most notably Modes 5 and 8, contained a varying degree of flattened posterior soft tissue artefacts associated with support to the calf and thigh as the participants lay supine. These modes were retained in the model because they were not influenced by particular outlying training shapes, and might be useful for correcting such variation.

A particular challenge associated with this SSM arose from its representation of partial anatomy, which required a novel approach to size normalization. However, absolute size is also important to clinical considerations. For example, the generally agreed shortest useful residual limb is defined anatomically: it needs to include the tibial tubercle so that knee extension is preserved (Carvalho et al., 2012). The surgical community recommends against transtibial amputation with less than about 3 cm of residual tibia (Pant and Younge, 2003), though this is unlikely to provide adequate load transfer in a socket. Clinical prosthetics guidance states at least 8 cm of tibia is required below the knee joint for socket use (Congdon, 2011), and propose the ideal length is 12.5–17.5 cm (Mollano, 2013), with some guidelines offering a proportional measure, at 2.5 cm residuum length per 30 cm of body height (Ertl, n.d.). Similarly, while longer residual limbs are preferred to preserve function and optimize gait rehabilitation (Majumdar et al., 2008), sufficient space is needed for prosthetic ankle–foot units which have build heights that can vary between 12 and 30 cm (Gabert et al., 2020), and this may make a very low amputation level impractical. Additionally, long transtibial amputation may not be advised due to poor blood supply to the distal end and insufficient soft tissue for closure. While various descriptions of what constitutes a "short" residual limb versus "medium" and "large" are used, both in % and cm, there is often a wide range between these definitions when applied with "long" often being anything from 50% to Symes level, a through-ankle technique that was excluded from this study. Especially when trying to navigate anatomical features such as muscle and nerves, there may be many amputation levels that are either impossible or impractical. Therefore, in extending this study to include individuals who do not lie on continuous spectra of variance, it may be necessary to use different sampling techniques or SSM dimensionality reduction methods.

Principal component analysis is considered the standard approach used for creating statistical shape models (Stegmann and Delgado Gomez, 2002). Barratt et al. created SSMs of the femur and pelvis using PCA, but discussed how independent component analysis (ICA) may have improved accuracy, particularly as it does not assume Gaussian distribution of data and can identify local variations independent from global shape (Barratt et al., 2008). However, ICA does not provide a unique set of modes, nor are they ordered by the described variation, making it unsuitable in this case. Ballester et al. proposed principal factor analysis (PFA) as an alternative to PCA. PFA models covariance between data rather than the total variance and can be easier to interpret (Ballester et al., 2005), however, PCA was selected for this study because it is better suited for predicting data.

4.2. Limitations

The primary limitation of this model is the relatively small sample size. The general trends of variance were similar to the nearest comparable models available, which feature skin-only or prosthetic socket shapes. The substantial influence exerted by individual shapes indicate that the training dataset size is not sufficient to identify with confidence the *extremes* of shape variance in the general population. However, leaving out individual training shapes did not materially change the shape variations described by the first 10 principal modes which contained 95% of shape variation— and of the highest variance Modes, Mode 1 always represented length and Mode 2 always represented slender to bulbous soft tissue profile— which implies that the model can be trusted to describe the broader population trends. Quantitatively, the model's limited generality is observed where training shapes 10 and 20 substantially influenced the Mode 1 longest extreme shape (Figure 7, Table 2). With a small dataset it is difficult to confidently describe a value as an

https://doi.org/10.1017/dce.2025.10019 Published online by Cambridge University Press

outlier. However, we also do not know whether the data are continuous between this and the next closest subject, or whether indeed the population variance is continuous between any shapes. One example of discontinuous variance could arise from different surgical techniques, whose choice includes factors such as the extent of injury or disease, reason for amputation, and surgeon's specialty (Sebekos et al., 2023). The training shapes all come from high-income countries (UK, Germany, Australia and USA), three of which have universal health care that rank closely for quality (Schneider et al., 2021), and use similar surgical guidelines. However, training shapes 10 and 20 represent 60% and 51% of the full tibia, respectively, whereas the rest represented 18–46%, and alongside the amputation height guidance described earlier, this may indicate that an alternative amputation method was used and individual 10 lies within a different distribution with respect to amputation height or residual limb length. Other sources of discontinuous variance might arise from gender, with the training dataset primarily male, and from ethnocultural dimensions. There is some diversity within the training population, who are all from high-income countries, but black/African American and Asian ethnicities are under-represented and not described, respectively. Bony anatomy and soft tissue composition vary between ethnic groups and many geographic factors such as causes of amputation, surgical techniques, and lifestyle differences will affect the residual limb anatomy (Zengin et al., 2016; Yuan et al., 2023). The extent of variation between ethnic groups may dictate whether a model can be constructed which describes multiple ethnicities or ecogeographic groupings, or if separate models are required to avoid data bias.

4.3. Conclusions

This study presents a novel statistical shape model (SSM) describing a population of transtibial residual limbs derived from a sparse dataset of MRI and CT scans derived from five previously published cohorts. The model demonstrates the potential to predict internal bone shapes from external skin surface scans.

Approximately 52% of residual limb shape variance was attributed to amputation height, with soft tissue profile contributing a further 17%, and these observations are in line with the nearest equivalent statistical shape models which considered the limb surface only. In cross-validation, leave-one-out testing influenced the model's mean shape by between 0.14 and 0.88 mm RMSE surface deviation, and mode extreme shapes were accurate to below 9.00 mm for outlying training datasets, and 0.70 mm on average. Left-out shapes were recreated with RMSE from 1.8 to 5.7 mm.

Predicting bone shapes from skin surface scans provides value since limb surface scanning is part of routine clinical practice, but volume imaging is not. The current model demonstrates an average 6.7 mm (range 3.6–10.9 mm) RMSE of bone prediction, comprising both shape and position error, which may be improved by expanding the training dataset and incorporating probabilistic methods. We share both the model and methodology for processing data to include in it, with the aim of generating wider community action to expand this OpenLimbTT model. The development of such a residual limb statistical shape model which includes bone geometry holds potential for advancing prosthetic biomechanics research, and for facilitating the use of simulation to support evidence-based prosthetic socket design in the clinic.

Data availability statement. All data generated during the study have been made openly available from the University of Southampton repository at https://doi.org/10.5258/SOTON/D2895, on a CC-BY 4.0 license. The full OpenLimbTT model has been made openly available at https://github.com/abel-research/OpenLimbTT on a CC-BY-SA 4.0 license. Raw datasets analyzed during the study under secondary data analysis ethics approval cannot be made publicly available for reasons of individual privacy and/or under the terms of data sharing agreements under which they were included in this study. Requests to access these datasets should be directed to researchdata@soton.ac.uk.

Acknowledgments. At the time of writing, the OpenLimb Group includes Jennifer Bramley, Alex Dickinson, Cheryl Metcalf, Adam Sobey, Joshua Steer, Fiona Sunderland, and Peter Worsley (University of Southampton, UK), Rami Al-Dirini (Flinders University, Australia), Reza Safari (University of Derby, UK), Graci Finco (Baylor College of Medicine, USA), Ziyun Ding (University of Birmingham), Anthony Bull, Diana Toderita and David Henson (Imperial College London, UK), and Arjan Buis (University of Strathclyde, UK).

Author contribution. Fiona Sunderland contributed to formal analysis, investigation, methodology, software, validation, visualization, and writing—original draft. Adam Sobey, Cheryl Metcalf contributed to methodology, supervision, writing—original draft

and review and editing. Jennifer Bramley, Joshua Steer, Diana Toderita, Anthony Bull, Ziyun Ding, David Henson contributed to resources and writing—review and editing. Rami Al-Dirini and Peter Worsley contributed to conceptualization, methodology, resources, and writing—review and editing. Alex Dickinson contributed to conceptualization, data curation, formal analysis, investigation, methodology, project administration, resources, supervision, visualization, writing—original draft and review and editing.

Funding statement. This work was supported by the UK Engineering and Physical Sciences Research Council (EPSRC) grant EP/S02249X/1 for the Centre for Doctoral Training in Prosthetics and Orthotics, the UK Royal Academy of Engineering (RAEng) grant RF/130, the Lloyd's Register Foundation through Data-Centric Engineering, and the Royal British Legion. The Free Access Decedent Database was funded by the US National Institute of Justice grant number 2016-DN-BX-0144. The funders had no role in the design of the study; in the collection, analyses, or interpretation of data; in the writing of the manuscript, or in the decision to publish the results.

Competing interests. The authors have no competing interests to declare.

Adherence to ethical guidelines. This study was conducted according to the guidelines of the Declaration of Helsinki, and approved by the Institutional Ethics Committee of University of Southampton (protocol code ERGO 65748) as a secondary data analysis. All participants provided informed consent in the primary data collection studies cited in the text.

References

Abraham A, *et al.* (2014) Machine learning for neuroimaging with scikit-learn. *Frontiers in Neuroinformatics 8*, 14https://doi.org/10.3389/fninf.2014.00014.

Ambellan F, **Lamecker H**, **von Tycowicz C and Zachow S** (2019) Statistical shape models: Understanding and mastering variation in anatomy. *Advances in Experimental Medicine and Biology 1156*, 67–84. https://doi.org/10.1007/978-3-030-19385-0_5.

Amberg B, **Romdhani S and Vetter T** (2007) Optimal step nonrigid ICP algorithms for surface registration. *2007 IEEE Conference on Computer Vision and Pattern Recognition*, Minneapolis, MN, USA, 1–8. https://doi.org/10.1109/CVPR.2007.383165.

Audenaert EA, **Pattyn C**, **Steenackers G**, **De Roeck J**, **Vandermeulen D and Claes P** (2019) Statistical shape Modeling of skeletal anatomy for sex discrimination: Their training size, sexual dimorphism, and asymmetry. *Frontiers in Bioengineering and Biotechnology 7*, 302. https://doi.org/10.3389/fbioe.2019.00302.

Ballester MAG, **Linguraru MG**, **Aguirre MR and Ayache N** (2005) On the adequacy of principal factor analysis for the study of shape variability. *Proc. SPIE 5747, Medical Imaging 2005: ImageProcessing*, USA, 1392–1399. https://doi.org/10.7892/boris.61089.

Barratt DC, *et al.* (2008) Instantiation and registration of statistical shape models of the femur and pelvis using 3D ultrasound imaging. *Medical Image Analysis 12*(3), 358–374. https://doi.org/10.1016/j.media.2007.12.006.

Blanc R, **Seiler C**, **Székely G**, **Nolte LP and Reyes M** (2012) Statistical model based shape prediction from a combination of direct observations and various surrogates: Application to orthopaedic research. *Medical Image Analysis 16*(6), 1156–1166. https://doi.org/10.1016/J.MEDIA.2012.04.004.

Bramley J (2020) *Investigating the Mechanisms of Soft Tissue Damage at the Residual Limb-Socket Interface*. University of Southampton

Bui-Thanh T, **Damodaran M and Willcox K** (2004) Aerodynamic data reconstruction and inverse design using proper orthogonal decomposition. *AIAA Journal*. *42* (8), 1505–1516.

Carvalho JA, **Mongon MD**, **Belangero WD and Livani B** (2012) A case series featuring extremely short below-knee stumps. *Prosthetics and Orthotics International*. *36*(2), 236–238. https://doi.org/10.1177/0309364611430535.

Congdon W (2011) Standard of care: Lower extremity amputation. *The Brigham and Women's Hospital Inc.*, Department of Rehabilitation Services, MA, USA, 1–46.

Convery P, **Buis AWP**, **Wilkie R**, **Sockalingam S**, **Blair A and McHugh B** (2003) Measurement of the consistency of patellar-tendon-bearing cast rectification. *Prosthetics and Orthotics International 27*(3), 207–213. https://doi.org/10.1080/03093640308726683.

Costa A, **Rodrigues D**, **Castro M**, **Assis S and Oliveira HP** (2021) Embedding anatomical characteristics in 3D models of lower-limb sockets through statistical shape modelling. In *VISIGRAPP 2021—Proceedings of the 16th International Joint Conference on Computer Vision, Imaging and Computer Graphics Theory and Applications*. SciTePress, pp. 528–535. https://doi.org/10.5220/0010339805280535.

Dawson-Haggerty *et al.* (2019) Trimesh version 3.2.0. https://trimsh.org/

Dickinson A, **Diment L**, **Morris R**, **Pearson E**, **Hannett D and Steer J** (2021) Characterising residual limb morphology and prosthetic socket design based on expert clinician practice. *PRO 3*(4), 280–299. https://doi.org/10.3390/prosthesis3040027.

Dickinson AS, **Steer JW and Worsley PR** (2017) Finite element analysis of the amputated lower limb: A systematic review and recommendations. *Medical Engineering & Physics 43*, 1–18. https://doi.org/10.1016/j.medengphy.2017.02.008.

Dickinson AS, *et al.* (2022) Selecting appropriate 3D scanning Technologies for Prosthetic Socket Design and Transtibial Residual Limb Shape Characterization. *JPO Journal of Prosthetics and Orthotics 34*(1), 33–43. https://doi.org/10.1097/JPO.0000000000000350.

Ding Z, **Henson DP**, **Sivapuratharasu B**, **McGregor AH and Bull AMJ** (2023) The effect of muscle atrophy in people with unilateral transtibial amputation for three activities: Gait alone does not tell the whole story. *Journal of Biomechanics 149*, 111484. https://doi.org/10.1016/J.JBIOMECH.2023.111484.

Edgar H, **Berry SD**, **Moes E**, **Adolphi N**, **Bridges P and Nolte K** (2020) *New Mexico Decedent Image Database*. New Mexico

Ertl JP *Lower-Extremity Amputations Technique*. Medscape

Finco MG, **Finnerty C**, **Ngo W and Menegaz RA** (2023) Indications of musculoskeletal health in deceased male individuals with lower-limb amputations: Comparison to non-amputee and diabetic controls. *Scientific Reports 13*(1), 8838. https://doi.org/10.1038/s41598-023-34773-w.

Gabert L, **Hood S**, **Tran M**, **Cempini M and Lenzi T** (2020) A compact, lightweight robotic ankle-foot prosthesis: Featuring a powered polycentric design. *IEEE Robotics and Automation Magazine 27*(1), 87–102. https://doi.org/10.1109/MRA.2019.2955740.

Gariboldi F, *et al.* (2023) Mechanical testing of transtibial prosthetic sockets: A discussion paper from the American orthotic and prosthetic association socket guidance workgroup. *Prosthetics and Orthotics International 47*(1), 3–12. https://doi.org/10.1097/PXR.0000000000000222.

(2003) *Generalized Inverses*. New York: Springer-Verlag. https://doi.org/10.1007/b97366

Goh JCH, **Lee PVS**, **Toh SL and Ooi CK** (2005) Development of an integrated CAD–FEA process for below-knee prosthetic sockets. *Clinical Biomechanics 20*(6), 623–629. https://doi.org/10.1016/j.clinbiomech.2005.02.005.

Grassi L, **Väänänen SP and Isaksson H** (2021) Statistical shape and appearance models: Development towards improved osteoporosis care. *Current Osteoporosis Reports 19*(6), 676–687, https://doi.org/10.1007/s11914-021-00711-w.

Hafner BJ, **Zachariah SG and Sanders JE** (2000) Characterisation of three-dimensional anatomic shapes using principal components: Application to the proximal tibia. *Medical & Biological Engineering & Computing 38*(1), 9–16. https://doi.org/10.1007/BF02344682.

Keller M, **Zuffi S**, **Black MJ and Pujades S** (2022) OSSO: Obtaining skeletal shape from outside. In *2022 IEEE/CVF Conference on Computer Vision and Pattern Recognition (CVPR)*. IEEE, pp. 20460–20469. https://doi.org/10.1109/CVPR52688.2022.01984.

Lam A, **Garrison G and Rozbruch SR** (2016) Lengthening of tibia after trans-Tibial amputation: Use of a weight bearing external fixator-prosthesis composite. *HSS Journal 12*(1), 85–90. https://doi.org/10.1007/s11420-015-9463-7.

Lemaire ED and Johnson F (1996) A quantitative method for comparing and evaluating manual prosthetic socket modifications. *IEEE Transactions on Rehabilitation Engineering 4*(4), 303–309. https://doi.org/10.1109/86.547931.

Majumdar K, **Lenka P**, **Mondal R**, **Kumar R and Triberwala DN** (2008) Relation of stump length with various gait parameters in trans-tibial amputee. *Online Journal of Health and Allied Sciences 7* (2), 1–6.

Mbithi F *et al.* (2025) Evidence-Generated Sockets for Transtibial Prosthetic Limbs Compared With Conventional Computer-Aided Designs: Multiple-Methods Study From the Patient's Perspective. *JMIR Rehabil Assist Technol 12*, e69962. https://doi.org/10.2196/69962

Mendis MKS (2021) *Characterising Patient Specific Soft Tissue Deformation in the Residual Limb under Compressive Loads*. Flinders University

Mollano AV (2013) Standard below knee amputation. In Saghieh S, Weinstein SL and Hoballah JJ (eds), *Operative Dictations in Orthopedic Surgery*. New York: Springer New York, pp. 177–179. https://doi.org/10.1007/978-1-4614-7479-1_48

NHS England Secondary Care Analytical Team (2024), Hospital admitted patient care activity 2023-24, NHS Digital (https://digital.nhs.uk/data-and-information/publications/statistical/hospital-admitted-patient-care-activity/2023-24).

Oldfrey BM, *et al.* (2024) A scoping review of digital fabrication techniques applied to prosthetics and orthotics: Part 1 of 2—Prosthetics. *Prosthetics and Orthotics International*. https://doi.org/10.1097/PXR.0000000000000351.

Pant R and Younge D (2003) Turn-up bone flap for lengthening the below-knee amputation stump. *Journal of Bone and Joint Surgery—Series B 85*(2), 171–173. https://doi.org/10.1302/0301-620X.85B2.13252.

Pearson K (1901) LIII. On lines and planes of closest fit to systems of points in space. *The London, Edinburgh, and Dublin Philosophical Magazine and Journal of Science 2*(11), 559–572. https://doi.org/10.1080/14786440109462720.

Ramasamy E, *et al.* (2018) An efficient modelling-simulation-analysis workflow to investigate stump-socket interaction using patient-specific, three-dimensional, continuum-mechanical, finite element residual limb models. *Frontiers in Bioengineering and Biotechnology 6*, 126. https://doi.org/10.3389/fbioe.2018.00126.

Rogers AD and Khatib AE (2024) Surgical management of pressure-induced skin and soft tissue injuries. In: *UpToDate*, Colwell AS and Cochran A (Eds), Wolters Klower. (Accessed on July 28, 2025)

Safari MR and Meier MR (2015) Systematic review of effects of current transtibial prosthetic socket designs-part 1: Qualitative outcomes. *Journal of Rehabilitation Research and Development 52*(5), 491–508. https://doi.org/10.1682/JRRD.2014.08.0183.

Safari MR and Meier MR (2015) Systematic review of effects of current transtibial prosthetic socket designs—Part 1: Qualitative outcomes. *Journal of Rehabilitation Research and Development 52*(5), 491–508. https://doi.org/10.1682/jrrd.2014.08.0183.

Saxby DJ, *et al.* (2020) Machine learning methods to support personalized neuromusculoskeletal modelling. *Biomechanics and Modeling in Mechanobiology 19*(4), 1169–1185. https://doi.org/10.1007/s10237-020-01367-8.

Schneider EC, **Shah A**, **Doty MM**, **Tikkanen R**, **Fields K and Williams RD** (2021) Mirror, Mirror 2021—Reflecting poorly: Health Care in the U.S. compared to other high-income countries. https://doi.org/10.26099/01dv-h208.

Sebekos K, *et al.* (2023) Comparison of outcomes in below-knee amputation between vascular, general, and Orthopedic surgeons. *The Journal of Surgical Research 290*, 247–256. https://doi.org/10.1016/j.jss.2023.04.022.

Shetty K, *et al.* (2023) BOSS: Bones, organs and skin shape model. *Computers in Biology and Medicine 165*, 107383. https://doi.org/10.1016/J.COMPBIOMED.2023.107383.

https://doi.org/10.1017/dce.2025.10019 Published online by Cambridge University Press

Steer JW (2019) *Developing Parametric Finite Element Models of the Residual Limb—Prosthetic Socket System towards Clinical Application*. University of Southampton

Steer J, **Stocks O**, **Parsons J**, **Worsley P and Dickinson A** (2020) Ampscan: A lightweight python package for shape analysis of prosthetics and orthotics. *Journal of Open Source Software 5*(48). https://doi.org/10.21105/joss.02060.

Steer JW, **Worsley PR**, **Browne M and Dickinson AS** (2020) Predictive prosthetic socket design: Part 1-population-based evaluation of transtibial prosthetic sockets by FEA-driven surrogate modelling. *Biomechanics and Modeling in Mechanobiology 19*(4), 1331–1346. https://doi.org/10.1007/s10237-019-01195-5.

Steer JW, **Worsley PR**, **Browne M and Dickinson A** (2021) Key considerations for finite element modelling of the residuum–prosthetic socket interface. *Prosthetics and Orthotics International 45*(2), 138–146.

Stegmann MB and Delgado Gomez D (2002) *A brief introduction to statistical shape analysis*. Technical University of Denmark, Lyngby, Denmark, https://www2.imm.dtu.dk/pubdb/edoc/imm403.pdf

Trotter M and Gleser GC (1952) Corrigenda to "estimation of stature from long limb bones of American whites and negroes. *American Journal Physical Anthropology 47*(2), 355–356. https://doi.org/10.1002/ajpa.1330470216.

Woods C, **Fernee C**, **Browne M**, **Zakrzewski S and Dickinson A** (2017) The potential of statistical shape modelling for geometric morphometric analysis of human teeth in archaeological research. *PLoS One 12*(12), e0186754. https://doi.org/10.1371/journal.pone.0186754.

Worsley P, **Steer J**, **Christopher W and Dickinson A** (2015) Classifying residual limb shape in transtibial amputees. *Prosthetics and Orthotics International 39*(S1), 414. https://doi.org/10.1177/0309364615591101.

Wu G, *et al.* (2005) ISB recommendation on definitions of joint coordinate systems of various joints for the reporting of human joint motion--part II: Shoulder, elbow, wrist and hand. *Journal of Biomechanics 38*(5), 981–992. https://doi.org/10.1016/j.jbiomech.2004.05.042.

Yuan B, **Hu D**, **Gu S**, **Xiao S and Song F** (2023) The global burden of traumatic amputation in 204 countries and territories. *Frontiers in Public Health 11*, 1258853. https://doi.org/10.3389/fpubh.2023.1258853.

Zengin A, *et al.* (2016) Ethnic differences in bone geometry between white, Black and south Asian men in the UK. *Bone 91*, 180–185. https://doi.org/10.1016/j.bone.2016.07.018.

https://doi.org/10.1017/dce.2025.10019 Published online by Cambridge University Press

Appendix 1: Participant data

Table A1. *Description of training dataset participants and estimation of their residual tibia proportion*

Subject	Source	Age (years)	Height (m)	Estimated full tibia length (mm)	Measured residual tibia length (mm)	Residual tibia proportion
1 F	UK 1	46	1.68	370	130	0.35
2 M	UK 1	53	1.73	380	147	0.39
3 M	UK 1	36	1.88	436	156	0.36
4 M	UK 1	62	1.88	440	111	0.25
5 M	UK 1	25	1.65	343	122	0.36
6 M	UK 1	30	1.65	343	126	0.37
7 M	UK 1	54	1.80	410	75	0.18
8 M	Germany	65	1.70	371	85	0.23
9 M	Germany	67	1.69	368	102	0.28
10 M	Aus	64	1.63**	343	204	0.60
11 M	USA	66	1.68	376	88	0.23
12 M	USA	42	1.87*	429	196	0.45
13 M	USA	68	1.89	466	173	0.37
14 M	USA	79	1.83	419	150	0.36
15 M	USA	56	1.75	394	124	0.32
16 M	USA	66	1.74	409	108	0.27
17 M	USA	79	1.78	399	170	0.43
18 F	USA	59	1.61	352	142	0.40
19 M	USA	77	1.8	379	110	0.29
20 M	USA	39	1.8	415	213	0.51
21 M	USA	54	1.75	379	141	0.37
22 M	USA	81	1.7	374	108	0.29
23 M	USA	44	1.88	404	126	0.31
24 M	USA	48	1.75	387	152	0.39
25 M	USA	48	1.75	387	126	0.33
26 M	USA	58	1.78	400	146	0.37
27 F	USA	54	1.53	313	93	0.30
28 F	USA	68	1.55	329	77	0.24
29 M	UK 2	32	1.82	364	128	0.35
30 M	UK 2	32	1.76	352	162	0.46
31 M	UK 2	37	1.85	364	121	0.33
32 M	UK 2	33	1.77	320	143	0.45
33 M	UK 2	34	1.81	353	146	0.42
Median (range)		54 (25–81)	1.76 (1.53–1.89)	378 (313–466)	130 (77–213)	0.36 (0.18–0.60)

Note. Heights of some participants were not given, so were estimated using either *the contralateral tibia where available and intact, or **corresponding tibial landmarks of other participants.

Cite this article: Sunderland F, Sobey A, Bramley J, Steer J, Al-Dirini R, Metcalf C, Toderita D, Bull A, Ding Z, Henson D, the OpenLimb Group, Worsley P and Dickinson A (2025). OpenLimbTT, a transtibial residual limb shape model for prosthetics simulation and design: creating a statistical anatomic model using sparse data. *Data-Centric Engineering*, 6, e39. doi:10.1017/dce.2025.10019

https://doi.org/10.1017/dce.2025.10019 Published online by Cambridge University Press